Accepted Manuscript

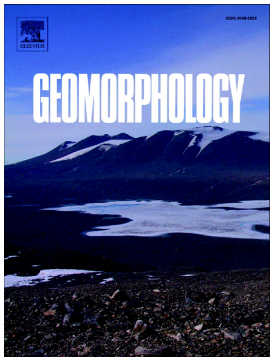

Age evaluation and causation of rock-slope failures along the western margin of the Antrim Lava Group (ALG), Northern Ireland, based on cosmogenic isotope (36Cl) surface exposure dating

David W. Southall, Peter Wilson, Paul Dunlop, Christoph Schnabel, Ángel Rodés, Pauline Gulliver, Sheng Xu

PII: S0169-555X(16)31109-6
DOI: doi: 10.1016/j.geomorph.2017.01.041
Reference: GEOMOR 5932

To appear in: *Geomorphology*

Received date: 21 November 2016
Revised date: 16 January 2017
Accepted date: 23 January 2017

Please cite this article as: David W. Southall, Peter Wilson, Paul Dunlop, Christoph Schnabel, Ángel Rodés, Pauline Gulliver, Sheng Xu , Age evaluation and causation of rock-slope failures along the western margin of the Antrim Lava Group (ALG), Northern Ireland, based on cosmogenic isotope (36Cl) surface exposure dating. The address for the corresponding author was captured as affiliation for all authors. Please check if appropriate. Geomor(2017), doi: 10.1016/j.geomorph.2017.01.041

Age evaluation and causation of rock-slope failures along the western margin of the Antrim Lava Group (ALG), Northern Ireland, based on cosmogenic isotope (^{36}Cl) surface exposure dating

David W. Southall[a], Peter Wilson[a*], Paul Dunlop[a], Christoph Schnabel[b], Ángel Rodés[b], Pauline Gulliver[c], Sheng Xu[d]

[a]*Environmental Sciences Research Institute, School of Geography and Environmental Sciences, Ulster University, Cromore Road, Coleraine, Co. Londonderry BT52 1SA, Northern Ireland, UK*

[b]*NERC Cosmogenic Isotope Facility, SUERC, Scottish Enterprise Technology Park, East Kilbride, Glasgow, G75 0QF, Scotland, UK*

[c]*NERC Radiocarbon Facility (Environment), SUERC, Scottish Enterprise Technology Park, East Kilbride, Glasgow, G75 0QF, Scotland, UK*

[d]*AMS Laboratory, SUERC, Scottish Enterprise Technology Park, East Kilbride, Glasgow, G75 0QF, Scotland, UK*

Main text: 6700 words.

*Corresponding author.
E-mail: P.Wilson@ulster.ac.uk

ABSTRACT

The temporal pattern of postglacial rock-slope failure in a glaciated upland area of Ireland (the western margin of the Antrim Lava Group) was evaluated using both ^{36}Cl exposure dating of surface boulders on run-out debris and ^{14}C dating of basal organic soils from depressions on the debris. The majority of the ^{36}Cl ages (~21-15 ka) indicate that major failures occurred during or immediately following local deglaciation (~18-17 ka). Other ages (~14-9 ka) suggest some later, smaller-scale failures during the Lateglacial and/or early Holocene. The ^{14}C ages (2.36-0.15 cal ka BP) indicate the very late onset of organic accumulation and do not provide close limiting age constraints. Rock-slope failure during or immediately following local deglaciation was probably in response to some combination of glacial debuttressing, slope steepening and paraglacial stress release. Later failures may have been triggered by seismic activity associated with glacio-isostatic crustal uplift and/or permafrost degradation consequent upon climate change. The ^{36}Cl ages support the findings of previous studies that show the deglacial - Lateglacial period in northwest Ireland and Scotland to have been one of enhanced rock-slope failure.

Keywords: rock-slope failures, ^{36}Cl surface exposure dating, ^{14}C dating, debuttressing, stress-release, palaeoseismicity, permafrost degradation

1. Introduction

Large-scale, relict rock-slope failures (RSFs) are conspicuous landscape features in many upland areas of former and current glaciation (Hewitt *et al*., 2008; Deline, 2009; Wilson, 2009; Shroder *et al*., 2011; Coquin *et al*., 2015; Nagelisen *et al*., 2015). Various styles of failure have been documented, namely rockslides, rock avalanches, in situ slope deformations, and rockfalls, and several triggering mechanisms proposed, including glacial erosion and subsequent debuttressing, rock stress reorganisation, seismicity, tectonic activity, and climatic changes, either singly or in some combinations (Jarman, 2006; Hewitt *et al*., 2008; McColl, 2012; Mercier *et al*., 2013). However, while some recent RSFs can reasonably be attributed to a specific recognisable trigger such as seismicity (Jibson *et al*., 2006; Owen *et al*., 2008), others cannot (Lipovsky *et al*., 2008; Stock *et al*., 2012) and such events may reflect the gradual crossing of stability thresholds in association with long-term deterioration in rock mass strength.

Sound arguments have been advanced in support of RSFs being a response to paraglacial (glacially conditioned) processes. Glaciation and deglaciation are regarded as factors that prepare slopes for subsequent failure by reducing rock mass stability through glacial erosion, and loading and unloading by glacier ice (Ballantyne, 2002; Cossart *et al*., 2008; McColl, 2012). These processes may trigger failure through stress release and associated extensional fracture development (Leith *et al*., 2014a, b). Additionally, in situ stresses may, over long time-scales, prepare rock slopes for failure as a result

of progressive joint propagation through intact rock bridges (Stock *et al*., 2012). Seismic activity and crustal uplift linked to deglaciation (Ballantyne *et al*., 2014a; Cossart *et al*., 2014), along with the thaw of bedrock permafrost (Allen *et al*., 2009; Lebrouc *et al*., 2013; Blikra and Christiansen, 2014) have also been proposed as key factors that can trigger RSFs.

Various methods have been used to assess the age of RSFs: e.g. ^{14}C dating of associated organic material (Pellegrini *et al*., 2004; Aa *et al*., 2007; Agliardi *et al*., 2009; Borgatti and Soldati, 2010), Schmidt hammer rebound measurements (Aa *et al*., 2007; Deline and Kirkbride, 2009; Wilson, 2009), tephrochronology (Berget, 1985; Hermanns and Schellenberger, 2008; Mercier *et al*., 2013), optically stimulated luminescence dating (Balescu *et al*., 2007; Pánek *et al*., 2011, 2012; Moreiras *et al*., 2015) and lichenometric dating (Owen *et al*., 2010). In addition, terrestrial cosmogenic nuclide surface exposure dating (TCND) has become a widely adopted technique for dating RSFs because the failure mechanism exposes fresh rock surfaces both on the rock wall and amongst the resulting debris (Cockburn and Summerfield, 2004; Hewitt *et al*. 2008). The method has been utilised by, for example, Hermanns *et al*. (2004), Mitchell *et al*. (2007), Ivy-Ochs *et al.* (2009), Stock and Uhrhammer (2010), Penna *et al*. (2011), Akçar *et al*. (2012), Ballantyne *et al*. (2014b), Zerathe *et al*. (2014) and Moreiras *et al*. (2015) and has provided valuable age constraints on individual RSFs and local RSF clusters. Pánek (2015) provides a recent review of progress in dating relict RSFs.

Temporal patterns of failure based on seismic stratigraphy, sea level curves, and/or ^{14}C dates have been investigated by Blikra *et al*. (2006) and Prager *et al*. (2008) for parts of the Norwegian fjords and Austrian Alps respectively. Peaks of RSF activity shortly after the last deglaciation (15-14 ka BP) in Norway, in the early Holocene (~10.5-9.4 ka BP) in the Alps, and in the later Holocene (~4.5-3.0 ka BP) in both regions, have been identified. A similar evaluation utilising a global dataset of published ^{14}C and TCND surface exposure ages, enabled McColl (2012) to recognise a clustering of RSF events in the early Holocene (10-8 ka) and the mid-to-late Holocene (3-2 ka). Each of these compilations demonstrates that while some RSFs occurred during or soon after local deglaciation, other slopes did not fail until several thousand years after ice retreat. A clustering of failure events in the southwestern Alps during the mid-Holocene (5.1-3.3 ka) has been demonstrated by Zerathe *et al*. (2014) through application of TCND. This timing along with the absence of recent local glaciation led the authors to associate the RSFs with an increased intensity of precipitation associated with the 4.2 ka BP climatic event.

TCND ages have been reported for several individual RSFs and small clusters of sites in the Highlands of Scotland and northwest Ireland (Ballantyne *et al*., 1998, 2009, 2013, 2014a; Ballantyne and Stone, 2004, 2009). Collation of 89 surface exposure ages from 31 RSFs enabled Ballantyne *et al*. (2014a) to assess the timing and periodicity of failure occurrence. The results indicate that RSFs occurred throughout almost the whole postglacial period from ~18-

17 ka until ~1.5 ka, but with failures ~4.6 times more frequent before ~11.7 ka than after that date. For sites deglaciated during retreat of the last ice sheet, peak RSF activity occurred ~1.6-1.7 ka after deglaciation but enhanced RSF activity lasted for ~5 ka after deglaciation, spanning the entire Lateglacial period.

To establish the temporal pattern of post-Last Glacial Maximum (LGM) rock-slope failure in a glaciated upland area of Northern Ireland we sampled for both ^{14}C dating and TCND (^{36}Cl) on three closely-spaced accumulations of coarse run-out debris at locations of uniform lithology (basalt) and structure. This strategy was designed to provide a robust test of the existing models by eliminating complicating issues such as a variable deglaciation age and non-uniform bedrock lithology.

2. Geological context

The Antrim Lava Group (ALG) of Northern Ireland is the largest extent of the North Atlantic Igneous Province in Britain and Ireland (Wilson and Manning, 1978; Cooper, 2004a). Basaltic lavas, extruded between 62 and 55 Ma ago, dominate the group and underlie an area of ~4000 km^2 (Fig. 1A). Borehole records indicate a maximum thickness for the lavas of ~880 m but exposures around the margin rarely exceed 100 m in thickness. The lavas are a strong cap over Cretaceous limestone and less competent Jurassic, Triassic and Carboniferous sedimentary successions; these underlying strata are seen in outcrop around the periphery of the lavas.

The onshore area occupied by the ALG rises to several broad summits of 300-550 m above sea level (asl) along parts of its eastern and western margins. The long-term evolution of the escarpments that bound the ALG has not been established but, as noted by Whittow (1975) and Davies and Stephens (1978), the lava plateau was probably considerably more extensive than defined by its present-day limits, as evidenced by detached fragments of the lavas to both north and south of the main body.

At different times during the Quaternary the area was invaded by ice sourced in western Scotland and from within Ireland. At a late stage during the last (Midlandian) glaciation, following retreat of lowland Irish ice, Scottish ice was able to advance up to several tens of kilometres across the north and northeast coasts of the lava plateau, incursions known respectively as the North Antrim Readvance and East Antrim Coastal Readvance. These readvances are inferred by McCabe and Williams (2012) to have occurred shortly after ~15.5 cal. ka BP immediately following the Killard Point Stadial (~16.5 cal. ka BP). The area to the north of Limavady (Fig. 1B) was apparently inundated by a lobe of ice associated with the North Antrim Readvance (McCabe *et al*., 1998; Bazley, 2004; McCabe, 2008) and therefore did not become ice free until ~15 cal. ka BP, although this is disputed by McCarron (2013). The timing of deglaciation for the area south of Limavady is not known with certainty, but McCarron (2013) associated the aggradation of substantial glaciolacustrine landforms in the Dungiven area with ice-sheet events related to Heinrich Event 1 at ~17.5 ka BP, suggesting that the area was still partially

ice-covered at that time. Directions of ice movement and associated timings are currently under review as part of the BRITICE-CHRONO project. (http://www.britice-chrono.group.shef.ac.uk)

It has been proposed that along the eastern and western edges of the ALG the weaker Cretaceous, Jurassic and Triassic strata beneath the basalt and limestone were severely eroded by glacier ice and that this resulted in large-scale slope failure (Prior *et al*., 1968; Davies and Stephens, 1978; Lewis, 1985; Cooper, 2004b; Knight, 2008). Davies & Stephens (1978) note that nowhere do the RSFs deform mid-Holocene raised beaches and contend this points to their stability over most of the postglacial period; Lewis (1985) thought that failure had probably occurred between deglaciation and the onset of the Lateglacial Interstadial at ~14.7 ka BP. However, no absolute dating of the RSFs had been undertaken. Although the RSFs are regarded as post-dating the Midlandian ice advances it is probably the case that earlier cycles of slope failure occurred during or subsequent to pre-Midlandian glacial events, similar to those discussed by Bentley and Dugmore (1998) for the basaltic rims of Icelandic glacial troughs and Jarman (2009) for troughs in the Scottish Highlands and Norway, with significant consequences for topographic evolution and progression.

3. Research area and sites

Along the western edge of its outcrop the ALG caps a west-facing escarpment for ~50 km south from the coast to Mullaghmore (550 m) (Fig. 1B). The base of the basalt rises irregularly from below sea level at the coast to over 400 m in the south. In plan, the scarp is divided into promontories and recesses in which deposits of glacial sediments extend to summit levels. The escarpment is cliffed along parts of the principal promontories (Binevenagh, Donalds Hill, Benbradagh and Mullaghmore). At the foot of the cliffs are a variety of landforms that result from large-scale slope failures; they extend up to 1.5 km from the present cliff line to about 200 m below the base of the basalt (Clark, 1984). The largest failed masses are the arrested translational blockslides on Binevenagh, with individual failed masses of ~1-3 M m^3. Below the other promontories the failed masses have undergone various degrees of fragmentation resulting in run-out debris with numerous surface boulders. These failures conform to the arrested translational slide and sub-cataclasmic categories of Jarman (2006) and it is with these latter sites, described below, that this paper is concerned.

3.1. Donalds Hill

The Donalds Hill RSF (also known as Donalds Pot, Irish Grid Reference C 739143) extends downslope for 500 m from 360 m asl at the highest point of the headscarp to 190 m asl at the lower margin of the debris lobe; the maximum width of the RSF is 470 m, across the base of the debris lobe. The

RSF (cavity and lobe) occupies an area of 0.15 km^2, of which 0.11 km^2 comprises failed material (Figs 2A and 3A).

Bedrock outcrops on the wedge-shaped headscarp (length 560 m, height 20-50 m) have numerous closely-spaced, cross-cutting fractures. The slope below the outcrops is predominantly boulder covered in the southeast, is vegetated in the central sector and has boulders and bare talus cones in the northwest. The debris lobe is largely vegetated and diversified by several (sub-) transverse ridges, benches and mounds. Surface boulders occur in scattered small clusters except in the southeast where they extend downslope, initially as a broad swathe, across the backslope and crest of the lobe and then as a narrowing tongue towards the lobe toe.

Based on profiles surveyed across the debris lobe and inferring a regular decline in the underlying slope gradient from above to below the lobe, the mean thickness of the failed material is estimated at 18 m. Lobe volume is calculated to be 1.33 M m^3, net, assuming a void space of one-third.

3.2. Benbradagh

At Benbradagh (C 720110) the central sector of a 4 km length of basalt scarp where evidence for RSFs is both extensive and varied in nature was investigated (Figs 2B and 3B). RSFs in this sector extend along the scarp for 2 km, and for 1.5 km downslope from 400 m OD to 120 m asl at the southern margin; the total area affected by failure is 2.1 km^2 of which 1.87 km^2 is run-out debris.

Headscarp character ranges from gullied basalt cliffs up to 30 m high interspersed with steep smooth vegetated embayments in which bedrock is generally concealed. The sinuous planform of the headscarp comprises several arcuate and wedge-shaped failure cavities, planar segments, and projecting buttresses. Slopes directly below the headscarp are mostly vegetated but gravel- to boulder-grade talus accumulations are also present.

The zone of run-out debris is of diverse form and thickness comprising up to 15 distinct boulder-dominated tongues that rise several metres above the adjacent terrain, they have steep (20-30°), high (3-7 m) frontal slopes and are laterally bounded by levee-like ridges (Fig. 3B). The size and morphology of these tongues, and the maximum dimensions of constituent boulders (*a* axes ~2-3 m) are suggestive of rapid downslope movement as a consequence of instantaneous headscarp failure rather than slow creep-like movement associated with periglacial blockslope accumulations. However, it cannot be demonstrated that all the run-out debris tongues are of the same age.

In the north, debris character is largely obscured by vegetation although infrequent exposures show that boulders are the dominant surface materials. Several convergent dry gullies cross part of this area. Farther south, and passing around the promontory of Benbradagh summit, debris accumulations are considerably more pronounced. On mid and upper slopes mega-blocks of slumped basalt with little apparent internal dislocation indicate scarp retreat of up to 130 m. Flanking and partly over-riding some of these blocks are lobate accumulations of steep-sided, open-work boulders and boulder sheets. On

lower slopes, lobate debris masses have been quarried and show angular basalt clasts with an infill of sand-rich material below 1-2 m depth.

The southern area, where the run-out zone reaches its maximum width, is a broadly-stepped slope of basalt mega-blocks and low-relief boulder tongues and sheets. Scarp retreat of at least 150 m is indicated by block widths. Several depressions upslope of blocks have accumulated organic-rich sediment up to 2 m in thickness. In places the lower margin of the RSF debris has been truncated by land reclamation (the foreground fields of Fig. 3B).

3.3. Mullaghmore

Rock-slope failures at Mullaghmore (C 735009) are present below a 3 km length of basalt scarp. The central 1.5 km of failure culminates at 500 m asl and extends downslope for a maximum distance of 0.9 km to 240 m asl. The area affected by failure is 1 km^2 of which 0.86 km^2 consists of run-out debris (Fig. 2C).

A prominent failure cavity with chord length of 220 m, depth of 40-50 m, and a partly cliffed and gullied headwall on its southern side dominates the headscarp (Figs 2C and 3C). North and south of the cavity the headscarp comprises either vegetated steep slopes with a few bedrock outcrops, or low (<20 m high) cliffs of fractured basalt.

Run-out debris below the cavity is characterised by ridges, benches and mounds of well-vegetated failed materials, many of which have an amplitude of 5-10 m, and extensive covers of large boulders. Depressions between ridges and mounds contain organic-rich sediment to 2 m thickness.

At a few locations secondary slope failure has occurred within the run-out debris. These sites are evidenced by distinct head and flank scarps up to 10 m high below which debris ridges, mounds and boulder spreads are present. Below ~350 m asl the run-out debris is considerably thinner than higher on the slope and there are outcrops of Carboniferous strata. These strata form prominent hillside terraces, particularly across the southern part of the run-out zone and passing into the forest, indicating that failed material from the headscarp is insufficiently thick to have obscured their outlines. Nevertheless, basalt boulder sheets extend across these terraces and their downslope termination was taken as the lower limit of the RSFs. As with Benbradagh, several episodes of rock-slope failure may be represented at Mullaghmore.

4. Field and laboratory methods

4.1. Sampling and ^{14}C measurement

Samples for ^{14}C dating were obtained from the basal sediments accumulated within each of eight shallow (<2 m deep) depressions on RSF debris (three at Benbradagh and five at Mullaghmore, Figs 1 and 3) in order to provide minimum ages for the failures. At each location the peat was probed with a metal rod to obtain a cross profile of the depression and to locate the

maximum thickness of organic soil. Pits were then excavated at these maxima locations and the lowermost 20 cm of organic soil was removed using monolith tins. In the laboratory the basal 1 cm was removed from each monolith and oven-dried at 100ºC prior to submission as 'bulk' samples for ^{14}C analysis. Three of the eight basal samples contained macrofossils which were isolated and submitted for ^{14}C analysis for comparison to ^{14}C content of associated bulk samples. Details of all samples are given in Table 1.

Bulk organic soils (samples SUERC-26059 to -26063 and -28815 to -28817) were lightly ground to disaggregate lumps and then sieved through 1 mm and 0.5 mm mesh sieves and the fine materials retained. Macrofossils (samples SUERC-26053 to -26055) were rinsed with deionised water to remove as much sediment as possible. Samples were then given a standard acid-alkali-acid pre-treatment at 80 ºC where the samples were sequentially digested in 2M HCl, 1M KOH, and 2M HCl. After each digestion samples were rinsed with de-ionised water. After the final HCl digestions samples were rinsed free of acid, dried and homogenised.

The total carbon in a known weight of the pre-treated sample was recovered as CO_2 by heating with CuO in a sealed quartz tube. Sample CO_2 gas was cryogenically purified and an aliquot converted to graphite by Fe/Zn reduction. $\delta^{13}C$ values were determined using a separate aliquot of sample CO_2 analysed on a dual inlet stable isotope mass spectrometer (VG OPTIMA), the quoted precision is the uncertainty of repeated measurements of the same CO_2 aliquot and represents machine uncertainty only.

In keeping with international practice ^{14}C results were corrected to $\delta^{13}C_{VPDB}$ -25‰ using the $\delta^{13}C$ values listed in Table 1 and are reported as conventional radiocarbon years BP (relative to AD 1950), expressed at the ±1σ level for overall analytical confidence (Stuiver and Polach, 1977). Calibration of the ^{14}C ages to calendar age ranges was performed using the OxCal on-line program (v.4.2) (Bronk Ramsey, 2009) and the INTCAL13 calibration dataset (Reimer *et al*., 2013). Age ranges (2σ) and their % probability values are provided in Table 1.

4.2. Sampling and ^{36}Cl measurement

TCND was applied to 18 samples from RSF run-out debris at Donalds Hill, Benbradagh and Mullaghmore. Samples were collected in accordance with recommended practices (Gosse & Phillips, 2001). At each location two sets of three samples were obtained; one set came from a site proximal to the RSF headscarp (sample numbers -04, -05, -06), the other (sample numbers -01, -02, -03) from a distal site (Figs 2, 4A and B). On the basis of field context these 'paired' sites were judged as comprising debris originating from the same area of headscarp. This strategy was employed to test for within- and between-site synchronicity of failure events. A sample of bedrock from the Mullaghmore headscarp (sample number -07) was also collected and analysed for ^{36}Cl, for comparison with the samples from run-out boulders.

Horizontal and near-horizontal upper surfaces of large (>1 m high) boulders were sampled using a hammer and chisel (Figs 4C and D). Sample locations and elevations were recorded with GPS and by reference to 1:50,000 scale maps. Topographic shielding was determined with compass and clinometer, sample thickness was measured with callipers, and rock density was calculated by displacement of sub-samples in water. The headscarp bedrock sample was taken from an exposure inclined at ~45º. Details of all samples are given in Table 2.

Crushed and sieved (<500 μm) samples were prepared for whole rock ^{36}Cl analysis by leaching twice in hot 2M HNO_3 (trace metal analysis grade) followed by thorough washing with ultrapure water to remove meteoric ^{36}Cl contamination from grain surfaces. Each sample was then split into two fractions: ~2 g for elemental analysis by Prompt-Gamma Neutron Activation Analysis (PGNAA) and ~20-24 g for analysis of ^{36}Cl with Accelerator Mass Spectrometry (AMS). Grains containing minerals of very high magnetic susceptibility were removed using a Frantz isodynamic magnetic mineral separator. Chlorine was extracted and purified from the 125-250 μm fraction of leached samples to produce AgCl for AMS analysis according to a modified version of procedures developed by Stone *et al*. (1996). High purity chemicals were used to minimize contamination with natural chloride and sulphur-containing compounds.

Samples were processed in batches of eight with each batch containing two full chemistry blanks. About 1.3 mg chloride enriched in ^{35}Cl was added

before dissolution in 1.3M HNO_3 (trace metal grade) and 13% ultrapure HF. The solution containing the chloride was separated by centrifugation from the fluorides that formed during dissolution. Chloride was recovered from the sample solutions by precipitation of rough AgCl from hot solution (Stone *et al*., 1996). This AgCl was re-dissolved in aqueous NH_3 (14 wt%, optima) to remove sulphur compounds of Ag. Due to isobaric interference of ^{36}S with ^{36}Cl in the AMS measurements, saturated $Ba(NO_3)_2$ solution (99.999 wt % metal basis) was used to precipitate sulphur as $BaSO_4$. At least 36 hours were allowed for $BaSO_4$ to settle from a cold solution (4 °C) in the dark before removal by filtration. Pure AgCl was re-precipitated by acidifying $[Ag(NH_3)_2]^+$ Cl^- solution with 5M nitric acid (optima). Finally, AgCl was recovered, washed and dried. It was then pressed into high-purity AgBr (99.9% metal basis, Alfa Aesar) in 6 mm diameter Cu-target holders. AgBr has been found to have much lower sulphur content than Cu. AgCl recovery from three samples (DON-01, MULL-01 and -03) was insufficient for an AMS measurement and therefore these are not considered further.

The $^{36}Cl/^{35}Cl$ and $^{36}Cl/^{37}Cl$ ratios were measured with the SUERC 5 MV accelerator mass spectrometer (Wilcken *et al*., 2010); gas stripping (for good brightness/low ion straggling) to the 5+ charge-state suffices for effective interference separation combined with sample-efficient and rapid analysis. The Purdue Z93-0005 (nominally 1.20 x 10^{-12} $^{36}Cl/Cl$) AMS primary normalization standard is long-term consistent (Wilcken *et al*., 2010) with the secondary standard (nominally 5.0 x 10^{-13} $^{36}Cl/Cl$; Sharma *et al*., 1990) used

for assessing overall uncertainties. Corrections for ^{36}Cl measured in blanks prepared together with the samples (the average of the two fully processed blanks containing ~3.10^{-14} ^{36}Cl/Cl within a batch was used for the respective samples) ranged between 3 and 32%.

PGNAA is appropriate for the determination of the target elements affecting the production of ^{36}Cl in rocks (Gméling *et al*., 2005; Di Nicola *et al*., 2009). Thus, the concentrations of the target elements for ^{36}Cl production, Cl, K, Ca, Ti and Fe, were determined with PGNAA in the Nuclear Research Department, Institute of Isotopes, HAS, Budapest together with concentrations of neutron absorbers, such as B, Sm and Gd, the neutron moderator H and major elements (Tables S1 and S2).

The ^{36}Cl ages were calculated according to the production rates given by Marrero *et al*. (2016) through the CRONUS-Earth ^{36}Cl Exposure Age Calculator v.2.0 using the Lm scaling scheme. Exact values and uncertainties used are given in Table 3. No correction for post-depositional surface erosion was made.

5. Results

5.1. Calibrated ^{14}C ages

All samples submitted for ^{14}C analysis returned ages that, when calibrated, indicate organic soil formation in the enclosed depressions to have occurred from ~2.36 ka cal BP onwards (Table 1). For two of the three sites at Benbradagh from which bulk and macrofossil ages were determined (BEN-S1

and S3) the bulk sample ages are indistinguishable at 1σ confidence limits from the age of contained macrofossil material (BEN-S1: 0.501-0.315 ka cal BP, BEN-S1a: 0.499-0.314 ka cal BP; BEN-S3: 0.473-0.304 ka cal BP, BEN-S3a: 0.461-0.151 ka cal BP) giving confidence in the use of these age ranges to determine initiation of organic accumulation at those sites. At the third site with paired macrofossil and bulk organic soil results (MULL-S4) the bulk sample was significantly older than the associated macrofossil (MULL-S4: 0.536-0.334 ka cal BP, MULL-S4a: 2.36-2.16 ka cal BP). The explanation for this age discrepancy (of ~1.8 ka) is not known with certainty but one of two scenarios can be envisaged. The first is that the bulk age may be correct, with the macrofossil sample having penetrated from higher in the organic soil profile. The second is that the macrofossil age may be correct with the bulk sample comprising older humified organic material washed into the depression as organic soil accumulation commenced.

Irrespective of this disparity, the data indicates that organic soil initiation can be assigned to one of three periods: firstly, 2.36-2.16 ka cal BP represented by MULL-S4a; secondly, 1.52-1.18 ka cal BP, incorporating BEN-S2, MULL-S1, -S2 and -S5; and thirdly, 0.63-0.15 ka cal BP, incorporating BEN-S1, -S1a, -S3 and -S3a, and MULL-S3 and -S4. The clustering of ages into the second and third periods may indicate that for MULL-S4/4a the second scenario above is more likely correct.

5.2. ^{36}Cl exposure ages

The ^{36}Cl ages range from 47.9±3.65 ka (DON-03) to 9.0±1.84 ka (BEN-06) (Table 2). Three samples (DON-02: 31.7±4.8 ka, DON-03: 47.9±3.65 ka and BEN-03: 24.4±2.79 ka) returned ages that, within 2σ uncertainties, pre-date the timing of local deglaciation (~18-17 ka BP; McCabe *et al*., 1998; Bazley, 2004; McCabe, 2008, McCarron, 2013) following the LGM. These samples are considered to be influenced by ^{36}Cl inherited from pre-LGM exposure to cosmic radiation and consequently they are of no value in establishing the timing of the failure events. All other samples except BEN-06 (9.0±1.84 ka) returned ages that are statistically indistinguishable from the local deglaciation age at either 1σ or 2σ.

Following the exclusion of ages compromised by inheritance, between-sample age variation within each distal and proximal cluster of samples was assessed by a filtering procedure aimed at identifying consistent results within clusters yielding two or more apparently compatible ages. The reduced Chi-squared (χ^2_R) test was applied to determine whether cluster ages could be considered consistent with sampling from a single normally distributed age population (χ^2_R ~≤1), or whether outlier ages were present (χ^2_R >1; Balco, 2011; Applegate *et al*. 2012; Small and Fabel, 2016). This procedure identified two ages (DON-04: 12.9±2.11 ka and MULL-04: 14.2±1.39) that may be compromised by surface erosion, shielding by a former debris cover or, given their locations proximal to their respective headscarps, they may

represent younger additions of rockfall debris. These ages are indicated as outliers in Table 3.

The filtering process resulted in two samples from each of the four clusters tested being regarded as belonging to the same age population and the uncertainty-weighted mean age of each pair was taken as the best-estimate age for emplacement of the run-out debris at the respective sites (Table 3). The BEN-04 – -06 cluster gave two possible combinations of consistent ages (-04 and -05, and -05 and -06) because of the large uncertainty value associated with BEN-05. Mean ages are given for both pairings.

Samples MULL-02 and -07 are also considered in discussion below. Although MULL-02 is the only sample from its cluster to have yielded an age, it represents the distal sampling location at Mullaghmore, and MULL-07 is from bedrock exposed on the RSF headscarp.

6. Discussion

6.1. Implications and significance of the ^{14}C age determinations

Although environmental conditions favouring organic soil accumulation in upland areas of Northern Ireland have prevailed from at least the mid-Holocene (Hall, 2011) ^{14}C ages from basal deposits in depressions on the RSF runout debris are considerably younger than the ^{36}Cl ages from surface boulders. The reason for this is unclear but we hypothesise that the run-out debris was sufficiently coarse that surface depression drained freely,

preventing sediment accumulation and organic soil development until sub-surface drainage routes became choked by fine clastic debris and organic materials washed from upslope. This did not happen until after ~1.5 ka BP. Thus, although the ^{14}C ages are minimum estimates for the timing of the RSF events, when considered in relation to the ^{36}Cl ages, they do not provide close limiting constraints. This finding is in marked contrast to the observations of Pánek (2015) who asserted that in most cases the age of peat on RSF debris is not normally significantly different from the timing of the RSF event (i.e. it is within dating uncertainties), but this may reflect the degree to which failure debris is open-work and freely/poorly drained.

6.2. Implications and significance of the ^{36}Cl age determinations

Three of the four sets of ^{36}Cl ages that yielded statistically consistent values have uncertainty weighted means of 17.89±1.79 ka, 16.52±3.17 ka and 17.67±1.52 ka (Table 3). These means also form a statistically consistent cluster ($\chi^2_R = 0.1$) with mean age of 17.36 ka. Taken at face value these data indicate that failure events at Donalds Hill, Benbradagh and Mullaghmore were broadly synchronous and most likely occurred as the sites were undergoing deglaciation. However, the ages for the Benbradagh proximal location present some difficulties with respect to their interpretation (see below).

At Donalds Hill, site morphology suggests a single episode of rock-slope failure occurred; based on proximal boulder ages this happened at 17.89±1.79 ka. Distal boulder ages are compromised by inheritance and these are likely to

have been part of the pre-failure scarp face in which some previously acquired ^{36}Cl remained due to insufficient glacial erosion.

The mean ages for the two groupings of proximal samples from Benbradagh indicate that failure occurred either in the Lateglacial period (BEN-04 and -05:13.13±2.27 ka) or the early Holocene (BEN-05 and -06: 9.22±1.73 ka). Alternatively, the range of ages may suggest slope failure activity spanning the Lateglacial to early Holocene.

At Mullaghmore, sample MULL-07 (15.70±2.02ka) from headscarp bedrock overlaps within 1σ limits with the weighted mean age from proximal debris samples MULL-05 and -06 (17.67±1.52ka) providing support for failure at ~18-16 ka. Sample MULL-02 (21.0±2.54 ka) from the distal component of the run-out debris overlaps at 1σ with the mean age from the proximal run-out debris (and also overlaps at 1σ with the ~17.9 ka age from Donalds Hill and at 2σ with the ~16.5 ka age from Benbradagh).

Until such time as more ages with higher precision become available we propose that the rock-slope failure debris at Donalds Hill (distal and proximal), Benbradagh (distal) and Mullaghmore (distal and proximal) most likely accumulated around ~18-16 ka, during or immediately following local deglaciation. At Benbradagh (proximal) the debris is likely younger, having accumulated during the Lateglacial or early Holocene periods. These timings have implications for the range of trigger mechanisms that are normally held responsible for rock-slope failure.

6.3. Trigger mechanisms

Several trigger mechanisms involving regional environmental changes (geological and climatic) have been proposed to explain RSFs. These mechanisms are not mutually exclusive; they may have operated in various combinations with different levels of influence.

6.3.1. Debuttressing, slope steepening and paraglacial stress release

Debuttressing refers to the removal of supporting glacier ice during deglaciation, a consequence of which may be the kinematic release of rock masses. Its role has been discussed by several authors (e.g. Ballantyne, 2002; Agliardi *et al*., 2009; Ivy-Ochs *et al*., 2009; Mercier *et al*., 2013; Cossart *et al*., 2014) although not all have regarded it as a key factor in rock-slope failure. Because the mean ages at Donalds Hill, Benbradagh (distal) and Mullaghmore overlap with the age of local deglaciation we consider that slope failure at all sites along the basalt scarp was probably in direct response to slope debuttressing. A similar conclusion was reached by Ballantyne *et al*. (2014a) with respect to 31 dated RSFs in the Highlands of Scotland and northwest Ireland.

In addition, glacial erosion may promote the destabilization of slopes by undercutting and steepening (McColl and Davies, 2013; Cossart *et al*., 2014) and this had been earlier proposed as an explanation for rock-slope failure along the margin of the ALG where undercutting had been favoured by outcrops of less competent Cretaceous, Jurassic and Triassic strata (Prior *et al*., 1968; Davies and Stephens, 1978; Lewis, 1985; Cooper, 2004b; Knight,

2008). Glacial undercutting and steepening of the basalt probably occurred and the temporal correspondence between the ^{36}Cl ages and deglaciation indicates that failure may have been a direct consequence of these effects.

Paraglacial stress release refers to the development of tensile stresses in rock slopes as a result of the unloading of and/or erosion by glacier ice (Ballantyne, 2002; McColl *et al*., 2010; McColl, 2012; Leith et al., 2014a, b) and it is widely accepted that it plays a major role in weakening slopes and preparing them for failure. In general, stress release is considered to facilitate internal fracture propagation and development of slope-parallel sheeting joints which may cause immediate or delayed failure depending on local rates of joint network development (Eberhardt *et al*., 2004; Cossart *et al*., 2008; Gugliemi and Cappa, 2010). In the ALG basalt the vertical joint network probably formed as the lava cooled but was likely to have undergone further extensional development during deglaciation. The rate of fracture propagation in the basalt of the ALG cannot be known but given its undoubted time-dependent nature and strength-reduction impact it cannot be entirely rejected as an intrinsic contributor to rock-slope failure. Progressive joint development was regarded by Ballantyne *et al*. (1998) as of critical importance in causing failure on a glaciated basalt scarp on the Isle of Skye, Scotland, ~10 ka after deglaciation.

Taken together or individually, debuttressing, slope steepening and paraglacial stress release are mechanisms widely regarded as capable of triggering rock-slope failure. The temporal pattern of the basalt RSFs strongly suggests that one or more of these mechanisms was involved.

6.3.2. Palaeoseismicity

Presently, Ireland lies along a passive continental margin and is regarded as an aseismic region (Musson, 2007). Nevertheless, low magnitude earth tremors are quite common around the head of Lough Swilly, Donegal, ~60 km west-southwest of the basalt escarpment. This seismicity is considered by Blake (2006) to be due to the extension into Donegal of the large and complex fault systems that cross the western Highlands of Scotland.

Enhanced seismotectonic activity may have been associated with deglaciation from LGM limits. In the Sperrin mountains, ~40 km south of the basalt RSFs, Knight (1999) has described metre-scale normal faulting in glacigenic sediments that he attributed to reactivation of pre-existing Caledonian lineaments by ice unloading following the LGM, and Ballantyne *et al*. (2014a) argued that maximum rock-slope failure activity in the Highlands of Scotland and northwest Ireland coincides generally with maximum rates of glacio-isostatic crustal uplift in the former area. From Arisaig, western Scotland, 230 km north of the basalt escarpment, maximum rates of crustal uplift coincided with the Lateglacial period ~15.7-12.7 ka BP (Firth and Stewart, 2000), suggesting the period was one of heightened seismicity. The

weighted mean age of 13.13±2.27 from BEN-04 and -05 falls within this period as do ages of 12.9±2.11 ka (DON-04) and 14.2±1.39 ka (MULL-04) suggesting that palaeoseismicity may have triggered a later phase of failure at all sites. However, evidence for high-magnitude seismic events in the Lateglacial period has proved elusive; it is advocated here on the basis of a 'coincidence of timing' and presently cannot be dismissed.

6.3.3. A climate-related mechanism

A range of proxy data indicates that marked fluctuations in temperature and precipitation have occurred since deglaciation and these have been suggested as possible trigger mechanisms for paraglacial rock-slope failure (McColl, 2012). Climatic transitions have been regarded as important with respect to the timing of RSFs, both in the past and at the present day (Grove, 1972; Alexandrowicz, 1997; Borgatti and Soldati, 2010; Ravanel and Deline, 2010; Huggel *et al*., 2012).

The $\delta^{18}O$ record of the NGRIP ice core indicates that the interval between the start of deglaciation, around 19-18 ka BP, and the opening of the Lateglacial Interstadial, at 14.7 ka BP, in the circum-North Atlantic, was probably one of sustained cold, continental climate (Svensson *et al*., 2006) in which permafrost aggraded. Climate proxies from western Europe indicate that a cold, arid and windy environment prevailed at that time. In Northern Ireland mean July temperatures were probably no higher than 10 °C, mean January temperatures were within the range -25 to -20 °C and mean annual

temperatures were ~-8 °C (Atkinson *et al*., 1987; Huijzer and Vandenberghe, 1998). Rockwalls probably remained frozen during and following deglaciation. From Lough Nadourcan, Donegal, ~70 km west-northwest from the basalt RSFs, organic sedimentation and chironomid-inferred mean July air temperatures indicate warming was underway by ~15.3 cal. ka BP (Watson *et al*., 2010). The weighted mean age of 13.13±2.27 ka (BEN-04 and -05), and ages of 12.9±2.11 ka (DON-04) and 14.2±1.39 (MULL-04) are coincident with this warming. In the NGRIP ice core this transition corresponds to a temperature rise of ~10 ºC and this occurred within a few years to several decades (Steffensen *et al*., 2008). At Lough Nadourcan the warming was ~6-7 ºC (Watson *et al*., 2010). Such a marked temperature shift would likely have resulted in the rapid degradation of permafrost raising the potential for RSF through the thaw of ice-bonded rockwall joints, and is supported by contemporary examples from Alpine regions (Allen *et al*., 2009; Hipp *et al*., 2014), and modelling studies (Krautblatter *et al*., 2013; Lebrouc *et al*., 2013). Therefore, the possibility that permafrost degradation was a contributory factor in later rock-slope failure along the basalt escarpment is one deserving of further investigation.

6.4. Wider significance

The weighted mean ages of the three RSFs lend support to earlier results from other areas of Ireland and Britain that indicate the deglacial and Lateglacial periods were times of enhanced rock-slope failure. Nine RSFs in Donegal, 90-

150 km west of the basalt escarpment, returned ^{10}Be exposure ages of 17.71±0.89 ka to 11.69±0.51 ka (Ballantyne *et al*., 2013). From the Isle of Jura, 150 km northeast of the escarpment, ^{10}Be ages imply that five RSFs occurred between 15.37±0.92 ka and 12.78±0.57 ka (Ballantyne *et al*., 2014b). Several other RSFs in the Highlands of Scotland have yielded similar ages (Ballantyne *et al*., 2014a). Together these ages demonstrate that peak failure occurred within ~1.6-1.7 ka of local deglaciation, and the basalt ages from Northern Ireland fit this pattern.

The only other basalt RSF subjected to TCND in Britain (The Storr, Isle of Skye) gave a weighted mean age of 6.08±0.49 ka (Ballantyne and Stone, 2013). This mid-Holocene age for failure is intriguing because the site is only 85 km north-northwest of Arisaig where maximum rates of glacio-isostatic crustal uplift, and by inference intensified seismicity, have been recorded for the Lateglacial period (Firth and Stewart, 2000). If uplift-induced seismic activity was the principal cause of the many RSFs in Scotland and Ireland (Ballantyne *et al*., 2014a) then rock-slope failure at The Storr ~10 ka after deglaciation is a major anomaly. This failure could perhaps be explained by a local collapse of the escarpment, subsequent to the main failure event. Some support for crustal uplift and palaeoseismic activity as triggering mechanisms for RSFs on basalt escarpments in Iceland shortly after deglaciation is provided by Mercier *et al*. (2013) and Cossart *et al*. (2014). Given the extent of basalt RSFs in both Northern Ireland and the Inner Hebrides of Scotland (isles of Skye and Mull) the existing TCND dataset requires augmenting before firm

conclusions can be drawn concerning failure events and the timing of regional environmental changes.

7. Conclusions

1. Fifteen rock samples from surface boulders among rock-slope failure run-out debris at three locations along the western margin of the Antrim Lava Group yielded TCND ages within the range 47.9±3.65 to 9.0±1.84 ka. A sample of bedrock from a headscarp outcrop returned an age of 15.7±2.02 ka. These ages are the first direct age determinations to be obtained from RSF run-out debris and headscarp outcrop in Northern Ireland.

2. Three of the ages pre-date the timing of local deglaciation following the LGM and are considered to be comprised by ^{36}Cl inherited from pre-LGM exposure to cosmic radiation. A further two ages may have been influenced by surface erosion or shielding by a former debris cover, or may represent debris associated with younger smaller-scale rockfall events

3. Of the remaining ages, three groupings, each of two ages, are internally statistically consistent. Weighted means of these groups of 17.89±1.79 ka, 16.52±3.17 ka and 17.67±1.52 ka indicate that rock-slope failure at each site occurred during or immediately following local deglaciation (~18-17 ka).

4. Support for the 17.67±1.52 ka timing of the rock-slope failure event at Mullaghmore is provided by the age from the headscarp bedrock of 15.70±2.02 ka.

5. The temporal pattern of rock-slope failure along the basalt escarpment strongly suggests that failure was primarily a response to some combination of glacial debuttressing, slope steepening and paraglacial stress release. In addition, palaeoseismicity and permafrost degradation may have been implicated in later, smaller-scale failures.

6. The ages of the three RSFs are similar to ages established for other RSFs in Scotland and northwest Ireland, and indicate that major failures probably occurred within ~2-3 ka following deglaciation. The results support the contention of earlier studies that the deglacial and Lateglacial periods in Ireland and Britain were characterised by enhanced rock-slope failure.

The TCND ages are the first to be obtained from basalt RSFs in Northern Ireland and their interpretation represents a significant advance in understanding the post-LGM evolution of landforms along the western margin of the ALG. However, we recognise the need for more ages from a greater range of locations in order to verify or refute the temporal relationships outlined above, and for comparison with results of other RSF dating studies drawn from areas inundated by the last British-Irish Ice Sheet.

Acknowledgements

DWS thanks the Department of Employment and Learning (DEL), Northern Ireland, for provision of a postgraduate studentship during the course of which this work was conducted. Research support for the ^{14}C and ^{36}Cl analyses was provided by the Natural Environment Research Council (Allocations: NRCF/1386.0409 and CIAF/9056.1008 respectively). We thank Colin Ballantyne and David Jarman for their helpful suggestions regarding improvements to the text, and the encouraging words of an anonymous reviewer. The diagrams were prepared for publication by Paul Dunlop and Kilian McDaid.

References

Aa, A.R., Sjåstad, J., Sønstegaard, E., Blikra, L.H., 2007. Chronology of Holocene rock-avalanche deposits based on Schmidt-hammer relative dating and dust stratigraphy in nearby bog deposits, Vora, inner Nordfjord, Norway. The Holocene 17, 955-964.

Agliardi, F., Costa, G.B., Zanchi, A., Ravazzi, C., 2009. Onset and timing of deep-seated gravitational slope deformations in the eastern Alps, Italy. Geomorphology 103, 113-129.

Akçar, N., Deline, P., Ivy-Ochs, S., Alfimov, V., Hajdas, I., Kubik, P.W., Christl, M., Schlüchter, C., 2012. The AD 1717 rock avalanche deposits in the upper ferret Valley (Italy): a dating approach with cosmogenic ^{10}Be. Journal of Quaternary Science 27, 383-392.

Alexandrowicz, S.W., 1997. Holocene dated landslides in the Polish Carpathians. In: Matthews, J.A., Brunsden, D., Frenzel, B., Gläser, B., Weiɞ , M.M., (eds). Rapid mass movements as a source of climatic evidence for the Holocene. Gustav Fischer Verlag, Stuttgart, 75-83.

Allen, S.K., Gruber, S., Owens, I.F., 2009. Exploring steep bedrock permafrost and its relationship with recent slope failures in the Southern Alps of New Zealand. Permafrost and Periglacial Processes 20, 345-356.

Applegate, P.J., Urban, N.M., Keller, K., Lowell, T.V., Laabs, B.J.C., Kelly, M.A., Alley, R.B., 2012. Improved moraine age interpretations through explicit matching of geomorphic process models to cosmogenic

nuclide measurements from single landforms. Quaternary Research 77, 293-304.

Atkinson, T., Briffa, K., Coope, G.R., 1987. Seasonal temperatures during the past 22,000 years in Britain, reconstructed using beetle remains. Nature 325, 587-591.

Balco, G., 2011. Contributions and unrealized potential contributions of cosmogenic-nuclide exposure dating to glacier chronology, 1990-2010. Quaternary Science Reviews 30, 3-27.

Balescu, S., Ritz, J-F., Lamothe, M., Auclair, M., Todbileg, M., 2007. Luminescence dating of a gigantic palaeolandslide in the Gobi-Altay mountains, Mongolia. Quaternary Geochronology 2, 290-295.

Ballantyne, C.K., 2002. Paraglacial geomorphology. Quaternary Science Reviews 21, 1935-2017.

Ballantyne, C.K., Stone, J.O., 2004. The Beinn Alligin rock avalanche, NW Scotland: cosmogenic ^{10}Be dating, interpretation and significance. The Holocene 14, 448-453.

Ballantyne, C.K., Stone, J.O., 2009. Rock-slope failure at Baosbheinn, Wester Ross, NW Scotland: age and interpretation. Scottish Journal of Geology 45, 177-181.

Ballantyne, C.K., Stone, J.O., 2013. Timing and periodicity of paraglaqcial rock-slope failures in the Scottish Highlands. Geomorphology 186, 150-161.

Ballantyne, C.K., Schnabel, C., Xu, S., 2009. Exposure dating and reinterpretation of coarse debris accumulations ('rock glaciers') in the Cairngorm Mountains, Scotland. Journal of Quaternary Science 24, 19-31.

Ballantyne, C.K., Stone, J.O., Fifield, L.K., 1998. Cosmogenic Cl-36 dating of postglacial landsliding at The Storr, Isle of Skye, Scotland. The Holocene 8, 347-351.

Ballantyne, C.K., Wilson, P., Schnabel, C., Xu, S., 2013. Lateglacial rock slope failures in north-west Ireland: age, causes and implications. Journal of Quaternary Science 28, 789-802.

Ballantyne, C.K., Sandeman, G.F., Stone, J.O., Wilson, P., 2014a. Rock-slope failure following Late Pleistocene deglaciation on tectonically stable mountainous terrain. Quaternary Science Reviews 86, 144-157.

Ballantyne, C.K., Wilson, P., Gheorghiu, D., Rodés, À., 2014b. Enhanced rock-slope failure following ice-sheet deglaciation: timing and causes. Earth Surface Processes and Landforms 39, 900-913.

Bazley, R.A.B., 2004. Quaternary. In: Mitchell, W.I., (ed.). The geology of Northern Ireland – our natural foundation. Geological Survey of Northern Ireland, Belfast; 211-226.

Bentley, M.J., Dugmore, A.J. 1998. Landslides and the rate of glacial trough formation in Iceland. Quaternary Proceedings 6, 11-15.

Berget, J.E., 1985. Tephrochronology of antislope scarps on an alpine ridge near Glacier Peak, Washington, U.S.A. Arctic and Alpine Research 17,143-152.

Blake, T., 2006. Measuring Ireland's earthquakes. Extractive Industry Ireland 2006, 78-81.

Blikra, L.H., Christiansen, H.H., 2014. A field-based model of permafrost controlled rockslide deformation in northern Norway. Geomorphology 208, 34-49.

Blikra, L.H., Longva, O., Braathen, A., Anda, E., Dehls, J.F., Stalsberg, K., 2006. Rock slope failures in Norwegian fjord areas: examples, spatial distribution and temporal pattern. In: Evans, S.G., Mugnozza, G.S., Strom, A., Hermanns, R.L., (eds). Landslides from massive rock slope failure. Springer, Dordrecht; 475-496.

Borgatti, L., Soldati, M., 2010. Landslides as a geomorphological proxy for climate change: a record from the Dolomites (northern Italy). Geomorphology 120, 56-64.

Bronk Ramsey, C., 2009. Bayesian analysis of radiocarbon dates. Radiocarbon 51, 337-360.

Clark, R., 1984. The basalt scarp. In: Wilson, P., Carter, R.W.G., (eds). North east Co. Donegal and north west Co. Londonderry. Field Guide 7, Irish Association for Quaternary Studies, Dublin; 49-53.

Cockburn, H.A.P., Summerfield, M.A., 2004. Geomorphological applications of cosmogenic isotope analysis. Progress in Physical Geography 28, 1-42.

Cooper, M.R., 2004a. Palaeogene extrusive igneous rocks. In: Mitchell, W.I., (ed.). The geology of Northern Ireland – our natural foundation. Geological Survey of Northern Ireland, Belfast; 167-178.

Cooper, M.R., 2004b. Geohazards. In: Mitchell, W.I., (ed.). The geology of Northern Ireland – our natural foundation. Geological Survey of Northern Ireland, Belfast, 291-298.

Cossart, E., Braucher, R., Fort, M., Bourlès, D.L., Carcaillet, J., 2008. Slope instability in relation to glacial debuttressing in alpine areas (Upper Durance catchment, southeastern France): evidence from field data and ^{10}Be cosmic ray exposure ages. Geomorphology 95, 3-26.

Cossart, E., Mercier, D., Decaulne, A., Feuillet, T., Jónsson, H.P., Sæmundsson, Þ., 2014. Impacts of post-glacial rebound on landslide spatial distribution at a regional scale in northern Iceland (Skagafjörður). Earth Surface Processes and Landforms 39, 336-350.

Coquin, J., Mercier, D., Bourbeois, O., Cossart, E., Decauline, A., 2015. Gravitational spreading of mountain ridges coeval with Late Weichselian deglaciation: impact on glacial landscapes in Tröllaskagi, northern Iceland. Quaternary Science Reviews 107, 197-213.

Davies, G.L.H., Stephens, N., 1978. Ireland. Methuen, London.

Deline, P., 2009. Interactions between rock avalanches and glaciers in the Mont Blanc massif during the late Holocene. Quaternary Science Reviews 28, 1070-1083.

Deline, P., Kirkbride, M.P., 2009. Rock avalanches on a glacier and morainic complex in haut Val ferret (Mont Blanc Massif, Italy). Geomorphology 103, 80-92.

Di Nicola, L., Schnabel, C., Wilcken, K.M., Gméling, K., 2009. Determination of chlorine concentrations in whole rock: comparisons between prompt-gamma activation and isotope dilution AMS analysis. Quaternary Geochronology 4, 501-507.

Eberhardt, E., Stead, D., Coggan, J.S., 2004. Numerical analysis of initiation and progressive failure in natural rock slopes – the 1991 Rand rockslide. International Journal of Rock Mechanics and Mining Sciences 41, 69-87.

Firth, C.R., Stewart, I.S., 2000. Postglacial tectonics of the Scottish glacio-isostatic uplift centre. Quaternary Science Reviews 19, 1469-1493.

Gméling, K., Harangi, Sz., Kasztovszky, Zs., 2005. Boron and chlorine concentration of volcanic rocks: an application of prompt gamma activation analysis. Journal of Radioanalytical and Nuclear Chemistry 265, 201-214.

Gosse, J.C., Phillips, F.M., 2001. Terrestrial in situ cosmogenic nuclides: theory and application. Quaternary Science Reviews 20, 1475-1560.

Grove, J.M., 1972. The incidence of landslides, avalanches and floods in western Norway during the Little Ice Age. Arctic and Alpine Research 4, 131-138.

Gugliemi, Y., Cappa, F., 2010. Regional-scale relief evolution and large landslides: insights from geotechnical analyses in the Tinée Valley (southern French Alps). Geomorphology 117, 121-129.

Hall, V., 2011. The making of Ireland's landscape since the ice age. The Collins Press, Cork.

Hermanns, R.L., Schellenberger, A., 2008. Quaternary tephrochronology helps define conditioning factors and triggering mechanisms of rock avalanches in NW Argentina. Quaternary International 178, 261-275.

Hermanns, R., Niedermann, S., Ivy-Ochs, S., Kubik, P., 2004. Rock avalanching into a landslide-dammed lake causing multiple dam failure in Las Conchas valley (NW Argentina) – evidence from surface exposure dating and stratigraphic analyses. Landslides 1, 113-122.

Hewitt, K., Clague, J.J., Orwin, J.F., 2008. Legacies of catastrophic rock slope failures in mountain landscapes. Earth-Science Reviews 87,1-38.

Hipp, T., Etzelmüller, B., Westermann, S., 2014. Permafrost in Alpine rock faces from Joutunheimen and Hurrungane, southern Norway. Permafrost and Periglacial Processes 25, 1-13.

Huggel, C., Clague, J.J., Korup, O., 2012. Is climate change responsible for changing landslide activity in high mountains? Earth Surface Processes and Landforms 37, 77-91.

Huijzer, B., Vandenberghe, J., 1998. Climatic reconstruction of the Weichselian Pleniglacial in northwestern and central Europe. Journal of Quaternary Science 13, 391-417.

Ivy-Ochs, S., Poschinger, A.V., Synal, H-A., Maisch, M., 2009. Surface exposure dating of the Flims landslide, Graubünden, Switzerland. Geomorphology 103, 104-112.

Jarman, D., 2006. Large rock slope failures in the Highlands of Scotland: characterisation, causes and spatial distribution. Engineering Geology 83, 161-182.

Jibson, R.W., Harp, E.L., Schulz, W., Keefer, D.K., 2006. Large rock avalanches triggered by the M 7.9 Denali Fault, Alaska, earthquake of 3 November 2002. Engineering Geology 83,144-160.

Knight, J., 1999. Geological evidence for neotectonic activity during deglaciation of the southern Sperrin Mountains, Northern Ireland. Journal of Quaternary Science 14, 45-57.

Knight, J., 2008. Deglaciation and paraglacial landsliding in the Antrim Glens: an example from Garron Point. In: Whitehouse, N.J., Roe, H.M., McCarron, S., Knight, J., (eds). North of Ireland: field guide. Quaternary Research Association, London; 129-136.

Krautblatter, M., Funk, D., Günzel, F.K., 2013. Why permafrost rocks become unstable: a rock-ice-mechanical model in time and space. Earth Surface Processes and Landforms 38, 876-887.

Lebrouc, V., Schwartz, S., Baillet, L., Jongmans, D., Gamond, J.F., 2013. Modeling permafrost extension in a rock slope since the Last Glacial Maximum: application to the large Séchilienne landslide (French Alps). Geomorphology 198, 189-200.

Leith, K., Moore, J.R., Amann, F., Loew, S., 2014a. Subglacial extentional fracture development and implications for Alpine valley evolution. Journal of Geophysical Research: Earth Surface 119, 62-81.

Leith, K., Moore, J.R., Amann, F., Loew, S., 2014b. In situ stress control on microcrack generation and macroscopic extentional fracture in exhuming bedrock. Journal of Geophysical Research: Solid Earth 119, 594-615.

Lewis, C.A., 1985. Periglacial features. In: Edwards, K.J., Warren, W.P., (eds). The Quaternary History of Ireland. Academic Press, London; 95-113.

Lipovsky, P., Evans, S., Clague, J., Hopkinson, C., Couture, R., Bobrowsky, P., Ekström, G., Demuth, M., Delaney, K., Roberts, N., Clarke, G., Schaeffer, A., 2008. The July 2007 rock and ice avalanches at Mount Steele, St. Elias Mountains, Yukon, Canada. Landslides 5, 445-455.

Marrero, S.M., Phillips, F.M., Caffee, M.W., Gosse, J.C., 2016. CRONUS-Earth cosmogenic ^{36}Cl calibration. Quaternary Geochronology 31, 199-219.

McCabe, A.M., 2008. Glacial geology and geomorphology: the landscapes of Ireland. Dunedin Academic, Edinburgh.

McCabe, A.M., Knight, J., McCarron, S., 1998. Evidence for Heinrich event 1 in the British Isles. Journal of Quaternary Science 13, 549-568.

McCabe, A.M., Williams, G.D., 2012. Timing of the east Antrim coastal readvance: phase relationships between lowland Irish and upland Scottish ice sheets during the last glacial termination. Quaternary Science Reviews 58, 18-29.

McCarron, S., 2013. Deglaciation of the Dungiven basin, north-west Ireland. Irish Journal of Earth Sciences 31, 43-71.

McColl, S.T., 2012. Paraglacial rock-slope stability. Geomorphology 153-154, 1-16.

McColl, S.T., Davies, T.R.H., 2013. Large ice-contact slope movements: glacial buttressing, deformation and erosion. Earth Surface Processes and Landforms 38, 1102-1115.

McColl, S.T., Davies, T.R.H., McSaveney, M.J., 2010. Glacier retreat and rock-slope stability: debunking debuttressing. In: Williams, A.L., Pinches, G.M., Chin, C.Y., Massey, C.I., (eds). Geologically active. Taylor and Francis, London; 467-474.

Mercier, D., Cossart, E., Decaulne, A., Feuillet, T., Jónsson, H.P., Sæmundsson, Þ. 2013. The Höfðahólar rock avalanche (sturzström): chronological constraint of paraglacial landsliding on an Icelandic hillslope. The Holocene 23, 432-446.

Mitchell, W.A., McSaveney, M.J., Zondervan, A., Kim, K., Dunning, S.A., Taylor, P.J., 2007. The Keylong Serai rock avalanche, NW Indian Himalaya: geomorphology and palaeoseismic implications. Landslides 4, 245-254.

Moreiras, S.M., Hermanns, R.L., Fauqúe, L., 2015. Cosmogenic dating of rock avalanches constraining Quaternary stratigraphy and regional neotectonics in the Argentine Central Andes (32° S). Quaternary Science Reviews 112, 45-58.

Musson, R.M.W. 2007. British earthquakes. Proceedings of the Geologists' Association 118. 305-337.

Nagelisen, J., Moore, J.R., Vockenhuber, C., Ivy-Ochs, S., 2015. Post-glacial rock avalanches in the Obersee Valley, Glarner Alps, Switzerland. Geomorphology 238, 94-111.

Owen, L.A., Kamp, U., Khattak, G.A., Harp, E.L., Keefer, D.K., Bauer, M.A., 2008. Landslides triggered by the 8 October 2005 Kasmir earthquake. Geomorphology 94, 1-9.

Owen, G., Hiemstra, J.F., Matthews, J.A., McEwen, L.J., 2010. Landslide-glacier interaction in a neoparaglacial setting at Tverrbytnede, Jotunheimen, southern Norway. Geografiska Annaler 92A, 421-436.

Pánek, T., 2015. Recent progress in landslide dating: a global review. Progress in Physical Geography 39, 168-198.

Pánek, T., Tábořík, P., Komárková, V., Hradecký, J., Šťastný, M., 2011. Deep-seated gravitational slope deformations in the highest parts of the Czech Flysch Carpathians: evolutionary model based on kinematic analysis, electrical imaging and trenching. Geomorphology 129, 92-112.

Pánek, T., Šilhán, K., Hradecký, J., Strom, A., Smolková, V., Zerkal, O., 2012. A megalandslide in the northern Caucasus foredeep (Uspenskoye, Russia): geomorphology, possible mechanism and age constraints. Geomorphology 177-178, 144-157.

Pellegrini, G.B., Surian, N., Urbinati, C., 2004. Dating and explanation of Late Glacial – Holocene landslides: a case study from the southern Alps, Italy. Zeitschrift für Geomorphology 48, 245-258.

Penna, I.M., Hermanns, R.L., Niedermann, S., Folguera, A., 2011. Multiple slope failures associated with neotectonic activity in the southern central Andes (37°-37°30´S), Patagonia, Argentina. Geological Society of America Bulletin 123, 1880-1895.

Prager, C., Zangerl, C., Patzelt, G., Brandner, R., 2008. Age distribution of fossil landslides in the Tyrol (Austria) and its surrounding areas. Natural Hazards and Earth Systems Science 8, 377-407.

Prior, D.B., Stephens, N., Archer, D.R., 1968. Composite mudflows on the Antrim coast of north-east Ireland. Geografiska Annaler 50A, 65-78.

Ravanel, L., Deline, P., 2010. Climate influence on rockfalls in high-Alpine steep rockwalls: The north side of the Aiguilles de Chamonix (Mont Blanc massif) since the end of the 'Little Ice Age'. The Holocene 21, 357-365.

Reimer, P., Bard, E., Bayliss, A., Beck, J.W., Blackwell, P.G., Bronk Ramsey, C., Buck, C.E., Cheng, H., Edwards, R.L., Friedrich, M., Grootes, P.M., Guilderson, T.P., Haflidason, H., Hajdas, I., Hatté, C., Heaton, T.J., Hoffmann, D.L., Hogg, A.G., Hughen, K.A., Kaiser, K.F., Kromer, B., Manning, S.W., Niu, M., Reimer, R., Richards, D.A., Scott, E.M., Southon, J.R., Staff, R.A., Turney, C.S.M., van der Plicht, J., 2013. Intercal13 and Marine13 radiocarbon age calibration curves 0-50,000 years cal BP. Radiocarbon 55, 1869-1887.

Sharma, P., Kubik, P.W., Fehn, U., Gove, H.E., Nishiizumi, K., Elmore, D., 1990. Development of ^{36}Cl standards for AMS. Nuclear Instruments and Methods B 52, 410-415.

Shroder, J.F., Owen, L.A., Seong, Y.B., Bishop, M.P., Bush, A., Caffee, M.W., Copland, L., Finkel, R.C., Kamp, U., 2011. The role of mass movement on landscape evolution in the central Karakoram: discussion and speculation. Quaternary International 236, 34-47.

Small, D., Fabel, D..2016. Was Scotland deglaciated during the Younger Dryas? Quaternary Science Reviews 145, 259-263.

Steffenson, J.P., Andersen, K.K., Bigler, M., Clausen, H.B., Dahl-Jensen, D., Fischer, H., Goto-Azuma, K., Hansson, M., Johnsen, S.J., Jouzel, J., Masson-Delmotte, V., Popp, T., Rasmussen, S.O., Röthlisberger, R., Ruth, U., Stauffer, B., Siggard-Andersen, M-L., Sveinbjörnsdóttir, A.E., Svensson, A., White, J.W.C., 2008. High-resolution Greenland ice core data show abrupt climate change happens in a few years. Science 321, 680-684.

Stock, G.M., Uhrhammer, RA. 2010. Catastrophic rock avalanche 3600 years BP from El Capitan, Yosemite Valley, California. Earth Surface Processes and Landforms 35, 941-951.

Stock, G.M., Martel, S.J., Collins, B.D., Harp, E.L., 2012. Progressive failure of sheeted rock slopes: the 2009-2010 Rhombus Wall rock falls in Yosemite Valley, California, USA. Earth Surface Processes and Landforms 3, 546-561.

Stone, J.O., Allan, G.L., Fifield, L.K., Cresswell, R.G., 1996. Cosmogenic chlorine-36 from calcium spallation. Geochimica et Cosmochimica Acta 60, 679-692.

Stuiver, M., Polach, H.A., 1977. Discussion: reporting of ^{14}C data. Radiocarbon 19, 355-363.

Svensson, A., Andersen, K.K., Bigler, M., Clausen, H.B., Dahl-Jensen, D., Davies, S.M., Johnsen, S.J., Muscheler, R., Rasmussen, S.O., Röthlisberger, R., Steffensen, J.P., Vinther, B.M., 2006. The Greenland

ice core chronology 2005, 15-42 ka. Part 2: comparison to other records. Quaternary Science Reviews 25, 3258-3267.

Watson, J.E., Brooks, S.J., Whitehouse, N.J., Reimer, P.J., Birks, H.J.B., Turney, C., 2010. Chironomid-inferred late-glacial summer air temperatures from Lough Nadourcan, Co. Donegal. Journal of Quaternary Science 25, 1200-1210.

Whittow, J.B. 1975. Geology and scenery in Ireland. Penguin Books, Harmondsworth.

Wilcken, K.M., Freeman, S.P.H.T., Dougans, A., Xu, S., Loger, R., Schnabel, C., 2010. Improved ^{36}Cl AMS at 5 MV. Nuclear Instruments and Methods B 268, 748-751.

Wilson, H.E., Manning, P.I. 1978. Geology of the Causeway Coast. Memoir, Geological Survey of Northern Ireland, Belfast.

Wilson, P., 2009. Storurdi: a Late Holocene rock-slope failure (sturzstrom) in the Jotunheimen, southern Norway. Geografiska Annaler 91A, 47-58.

Zerathe, S., Lebourg, T., Braucher, R., Bourlés, D., 2014. Mid-Holocene cluster of large-scale landslides revealed in the southwestern Alps by ^{36}Cl dating. Insight on an Alpine-scale landslide activity. Quaternary Science Reviews 90, 106-127.

Figure captions

Figure 1. A: Onshore extent of the Antrim Lava Group (shaded) in Northern Ireland and outline of study area. B: Areas of large-scale rock-slope failure along the western margin of the Antrim Lava Group..

Figure 2. Geomorphological maps of the RSFs on Donalds Hill (A), Benbradagh (B) and Mullaghmore (C), showing locations of samples for TCND. Ages are given in Table 3.

Figure 3. A: The RSF on Donalds Hill showing arcuate headscarp and hummocky surface of failed materials. **B**: The northern and central sectors of the Benbradagh RSF. **C**: The central sector of the Mullaghmore RSF showing headscarp cavity and ridges and mounds of failed materials.

Figure 4. A: Boulder-dominated run-out debris at the Mullaghmore TCND proximal site. **B**: Cluster of boulders at the Benbradagh TCND distal site. **C**: Boulder DON-05. **D**: Boulder BEN-05. Scale bar is 30 cm long.

Tables

Table 1. Radiocarbon dates from peat-filled depressions on RSF debris at Benbradagh and Mullaghmore.

Table 2. Details of samples for cosmogenic isotope (^{36}Cl) surface exposure dating.

Table 3. ^{36}Cl concentrations, production rates of ^{36}Cl from Ca, K, Cl, Ti and Fe, and uncorrected exposure ages. Uncertainties on exposure ages are internal uncertainties at one sigma. Samples DON-01, MULL-01 and -03 (Table 2) yielded insufficient AgCl for AMS measurement.

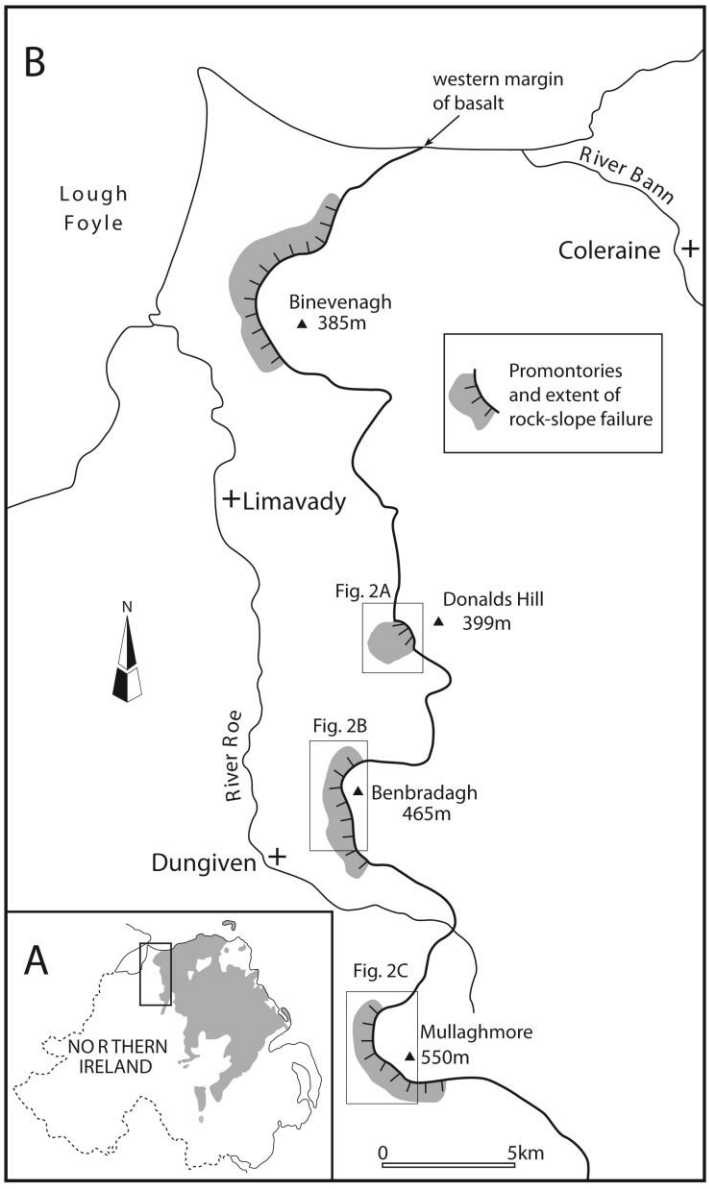

Fig. 1

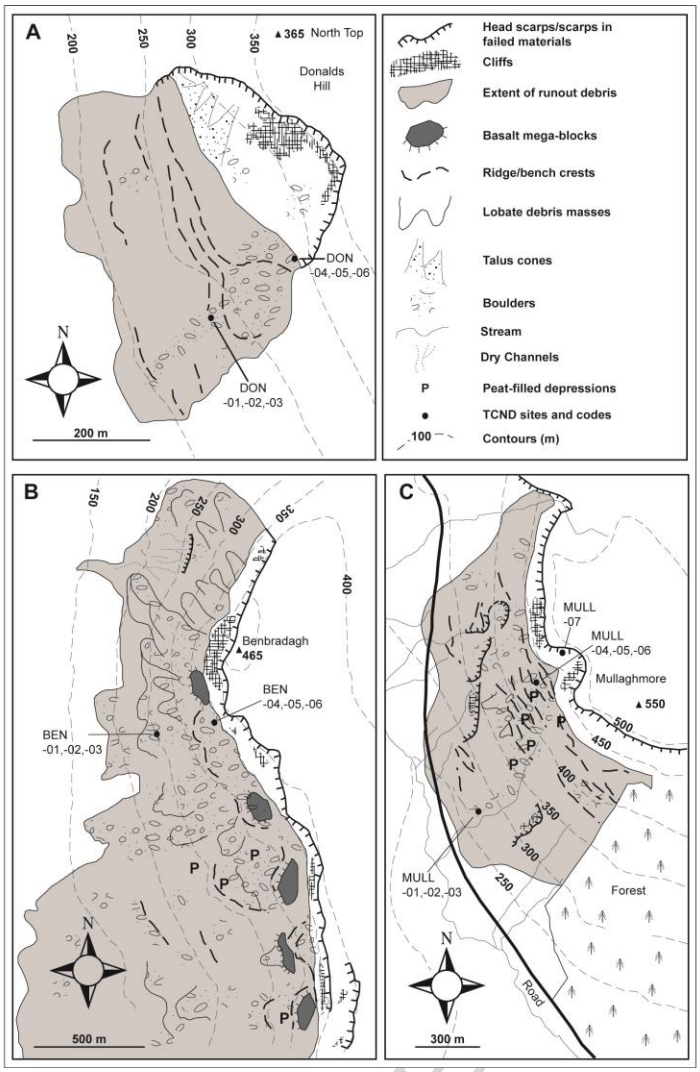

Fig. 2

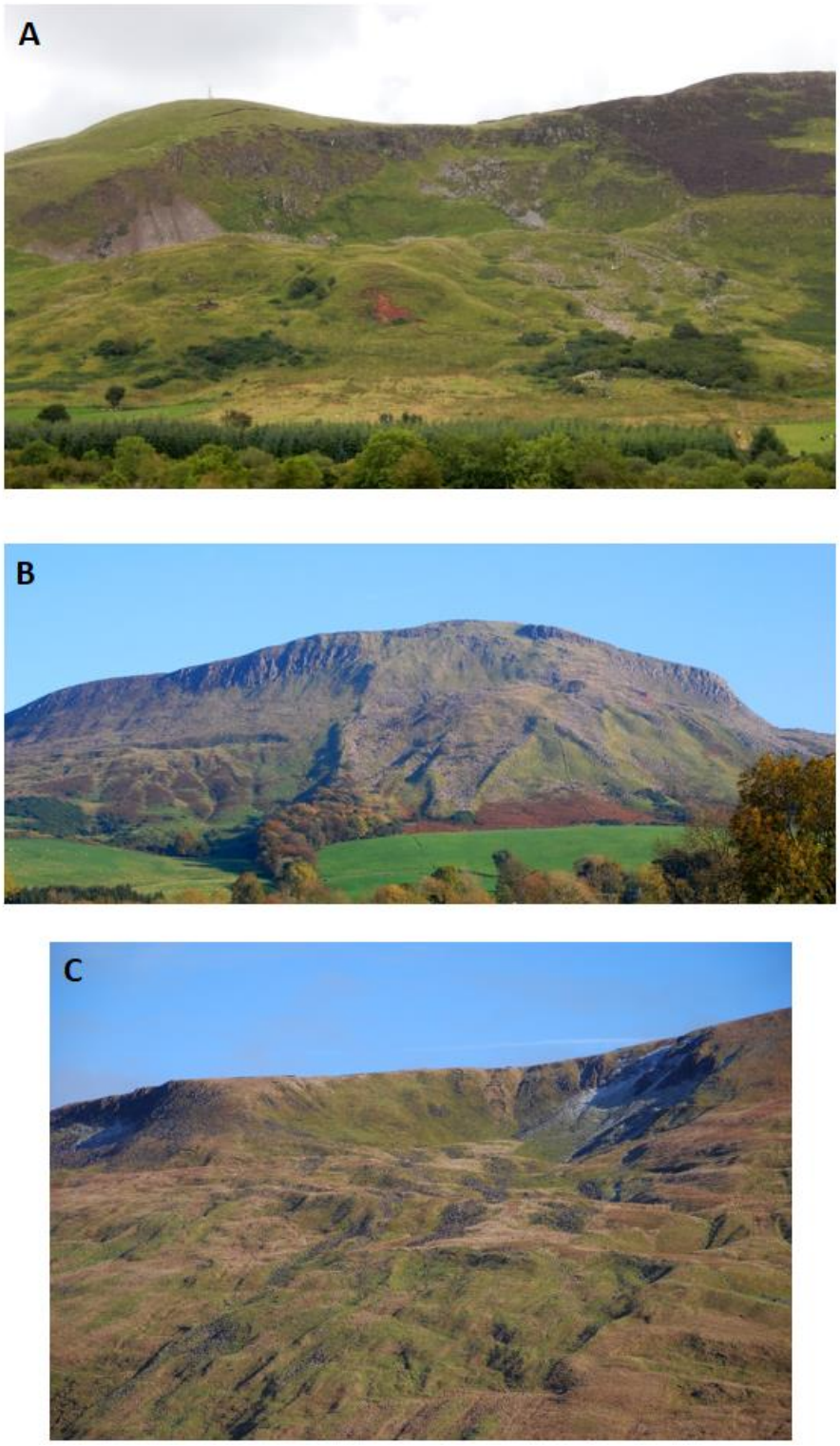

Fig. 3

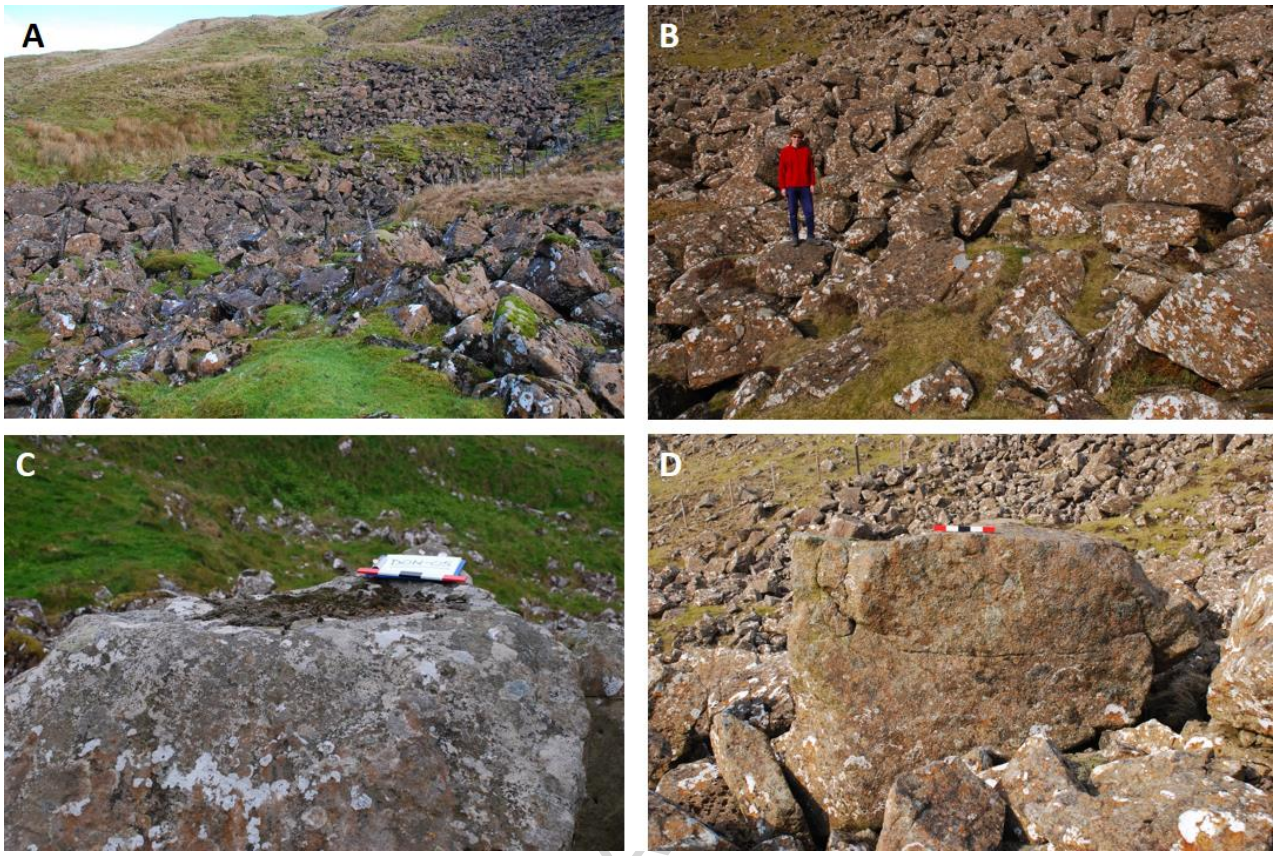

Fig. 4

Table 1. Radiocarbon dates from peat-filled depressions on RSF debris at Benbradagh and Mullaghmore.

Sample ID	Irish Grid Reference	Latitude (°N)	Longitude (°W)	Depth below surface (cm)	Laboratory code	Material	$\delta^{13}C_{VPDB}$ (‰) ±0.1	^{14}C age ± 1σ	Calibrated age: yr BP	Probability %
Benbradagh										
BEN-S1	C 721 105	54.931	6.869	125-126	SUERC-26053	Macrofossil (*Corylus* nutshell)	-25.9	363±37	501-420	47.7
									411-315	47.7
BEN-S1a	C 721 105	54.931	6.869	125-126	SUERC-28815	Peat - bulk	-29.6	358±37	499-418	45.3
									412-314	50.1
BEN-S2	C 723 104	54.935	6.873	50-51	SUERC-26059	Peat - bulk	-28.4	1336±37	1309-1223	77.4
									1213-1181	18.0
BEN-S3	C 724 098	54.936	6.875	80-81	SUERC-26054	Macrofossil (*Corylus* nutshell)	-26.2	321±35	473-304	95.4
BEN-S3a	C 724 098	54.936	6.875	80-81	SUERC-28816	Peat - bulk	-29.6	272±37	461-346	49.4
									339-280	38.3
									170-151	6.5
Mullaghmore										
MULL-S1	C 734 005	54.848	6.858	100-101	SUERC-26060	Peat - bulk	-28.7	1300±37	1294-1177	95.4
MULL-S2	C 735 007	54.848	6.857	150-151	SUERC-26061	Peat - bulk	-28.0	1538±37	1525-1352	95.4
MULL-S3	C 735 008	54.849	6.857	60-61	SUERC-26062	Peat - bulk	-28.9	521±37	632-598	19.0
									560-505	76.4
MULL-S4	C 735 009	54.850	6.856	75-76	SUERC-26055	Macrofossil (grass/ reed stems)	-25.9	438±35	536-438	91.2
									349-334	4.2
MULL-S4a	C 735 009	54.850	6.856	75-76	SUERC-28817	Peat - bulk	-28.4	2295±37	2360-2301	63.7
									2253-2160	31.7
MULL-S5	C 735 009	54.850	6.855	75-76	SUERC-26063	Peat - bulk	-29.3	1415±35	1375-1285	95.4

Table 2. Details of samples for cosmogenic isotope (^{36}Cl) surface exposure dating.

Sample ID	Irish Grid Reference	Latitude (°N)	Longitude (°W)	Altitude (m)	Thickness (cm)	Density (g cm^{-3})	Geographic scaling	Topographic shielding
Donald's Hill								
DON-01	C 739 171	54.9965	6.8449	235	3.8	2.94	1.276	0.983
DON-02	C 739 172	54.9968	6.8447	240	4.8	2.96	1.288	0.974
DON-03	C 739 172	54.9969	6.8445	240	4.4	2.93	1.301	0.992
DON-04	C 740 172	54.9976	6.8431	280	4.4	2.87	1.339	0.975
DON-05	C 740 172	54.9975	6.8430	280	1.0	2.77	1.339	0.986
DON-06	C 7401 72	54.9976	6.8431	280	5.0	2.82	1.339	0.983
Benbradagh								
BEN-01	C 718 109	54.9409	6.8801	270	4.0	3.29	1.326	0.990
BEN-02	C 718 109	54.9010	6.8798	270	3.5	3.13	1.326	0.985
BEN-03	C 718 109	54.9409	6.8798	270	4.3	3.05	1.326	0.983
BEN-04	C 720 110	54.9414	6.8762	360	4.5	3.00	1.450	0.984
BEN-05	C 720 110	54.9415	6.8763	355	6.0	3.22	1.437	0.984
BEN-06	C 720 110	54.9415	6.8763	355	5.0	3.06	1.437	0.984
Mullaghmore								
MULL-01	C 731 003	54.8456	6.8617	265	3.5	2.82	1.345	0.992
MULL-02	C 731 003	54.8456	6.8626	265	2.6	2.81	1.319	0.889
MULL-03	C 731 003	54.8455	6.8617	265	2.3	2.80	1.319	0.973
MULL-04	C 734 009	54.8514	6.8572	430	3.0	2.89	1.597	0.980
MULL-05	C 734 009	54.8515	6.8573	435	4.0	3.02	1.605	0.980
MULL-06	C 734 009	54.8514	6.8578	430	6.5	3.13	1.597	0.980
MULL-07	C 735 010	54.8518	6.8572	485	6.5	2.90	1.619	0.470

Table 3. ^{36}Cl concentrations, production rates of ^{36}Cl from Ca, K, Cl, Ti and Fe, and uncorrected exposure ages. Uncertainties on exposure ages are internal uncertainties at one sigma.
Samples DON-01, MULL-01 and -03 yielded insufficient AgCl for AMS measurement.

Sample ID	Lab ID for AMS	^{36}Cl conc. (10^5 atoms g^{-1})	PCa (atoms g^{-1} a^{-1})[a]	PK (atoms g^{-1} a^{-1})[a]	PCl (atoms g^{-1} a^{-1})[b]	PTi (atoms g^{-1} a^{-1})	PFe (atoms g^{-1} a^{-1})	P(slow muon) (atoms g^{-1} a^{-1})	Exposure age (ka)[c]	External uncertainty (ka)
Donald's Hill										
DON-02	c2363, c2364	1.674±0.187	4.17	0.49	0.40	0.05	0.12	0.24	31.70±4.80[d]	5.4
DON-03	c2365	3.047±0.133	4.28	0.53	1.46	0.06	0.13	0.25	47.90±3.65[d]	5.6
DON-04	c2366	0.685±0.088	4.23	0.37	0.35	0.06	0.16	0.21	12.90±2.11[e]	2.3
DON-05	c2367	0.955±0.091	4.37	0.51	0.40	0.06	0.16	0.2	17.10±2.12	2.5
DON-06	c2375	1.097±0.063	4.08	0.49	0.66	0.06	0.15	0.21	19.80±3.31	3.6
Weighted mean of DON-05 and -06									***17.89±1.79***	***2.05***
Benbradagh										
BEN-01	c2104, c2105	1.072±0.235	4.44	0.99	0.30	0.06	0.15	0.28	17.60±4.14	4.3
BEN-02	c2106, c2107	0.938±0.303	4.69	0.93	0.33	0.06	0.14	0.31	15.00±4.92	5
BEN-03	c2117	1.479±0.140	4.13	1.03	0.54	0.06	0.18	0.28	24.40±2.79[d]	3.3
Weighted mean of BEN-01 and -02									***16.52±3.17***	***3.26***
BEN-04	c2118, c2119	0.987±0.128	4.62	1.01	1.11	0.06	0.18	0.3	13.70±2.54	2.7
BEN-05	c2108, c2114	0.749±0.328	4.74	1.01	0.65	0.06	0.15	0.3	10.90±5.03	5.1
BEN-06	c2125, c2126	0.698±0.117	5.10	1.03	0.89	0.06	0.15	0.32	9.00±1.84	2
Weighted mean of BEN-04 and -05									***13.13±2.27***	***2.39***
Weighted mean of BEN-05 and -06									***9.22±1.73***	***1.86***

Mullaghmore										
MULL-02	c2383	1.131±0.068	4.02	0.55	0.57	0.05	0.13	0.23	21.00±2.54	3
MULL-04	c2387	0.870±0.038	4.67	0.54	0.49	0.07	0.20	0.25	14.20±1.39[e]	1.8
MULL-05	c2388	1.090±0.042	4.54	0.59	0.62	0.07	0.21	0.26	17.70±1.77	2.2
MULL-06	c2389	1.223±0.045	4.78	0.63	1.17	0.07	0.18	0.28	17.60±2.98	3.3
Weighted mean of MULL-05 and -06									***17.67±1.52***	***1.83***
MULL-07	c2394	0.459±0.027	2.17	0.23	0.33	0.03	0.11	0.12	15.70±2.02	2.3

[a] Marrero *et al.* (2016) for the Lm scheme.
[b] Muon production from Ca and K.
[c] Exposure ages calculated using the Lm scheme on the on-line calculator provided by Marrero *et al.* (2016)
[d] Sample age considered to be compromised by inheritance of ^{36}Cl.
[e] Outlier age - age that is not consistent with other ages from same cluster as determined by the reduced chi-squared (χ^2) statistic.